An Equilibrium Analysis of Magnetic Quadrupole Force Field with Applications to Microrobotic Swarm Coordination

Ioannis Faros and Herbert G. Tanner

***Abstract*— Controlled microrobots in fluidic environments hold promise for precise drug delivery and cell manipulation, opening new ways for personalized healthcare. However, coordinating magnetic microrobot swarms presents significant challenges due to the complexity of the associated actuation mechanisms. Given that there is no known method to exercise individual particle control within the magnetic microrobot swarm, the collective has to be steered as a whole, primarily by means of externally generated force fields. This paper contributes to an emerging set of methods that enable swarm control through manipulation of these force fields. This paper in particular exploits the nature of force field equilibria in a quadrupole workspace configuration as a means of steering the swarm while maintaining its cohesion. The approach also enables splitting the swarm in two subgroups in order to direct each simultaneously to a different location.**

I. INTRODUCTION

Controlled microrobots in suspension within fluidic environments have the potential to deliver drugs with pin-point accuracy, and manipulate individual cells, opening exciting new pathways for personalized healthcare, targeted drug delivery and potentially even contribute to by-design patient-compatible organ formation on demand. These systems have already seen applications in some aspects of drug delivery, biomedical engineering and cell manipulation [1]–[3]. One of the key challenges in this space, however, is that techniques for steering a single microrobot do not easily generalize to coordinated collections, or *swarms* [4], because of the physics of the actuation mechanisms and the fact that the robots themselves are too small to carry any meaningful sensing, computation, and independent actuation subsystems [5].

Some of the tools that have been used to steer magnetic micro-robots are microneedles, micropopettes, optical and *magnetic tweezers*. Among these tools, magnetic tweezers can propel specially designed magnetic microrobots by generating a magnetic field which exerts forces in a way that has desirable characteristics: (a) it avoids contact, and (b) enables motion with multiple degrees of freedom.

Magnetic tweezers can be categorized according to the number of the magnetic poles employed. For *quadrupole magnetic tweezers*, an analytical, physics-based force model relates the force on the magnetic particle with the currents applied to the tweezer coils [6]. Given that there is very limited capability to do any meaningful sensing or computation on the particle, all coordination is done externally, in a centralized fashion, primarily through the regulation of the coil currents. In this vein, a spectrum of microrobot control techniques have been explored, ranging from open loop control (i.e. combining their catalytic actuation with magnetic actuation [7]) to feedback control (i.e. deriving the sufficient currents for manipulations and stabilization [8]) with several variants in terms of the nature of the feedback control strategy. Almost invariably, these control strategies determine the tweezer coil currents in order to control the motion of the magnetic particles. In some other instances, the control is exerted through an additional (to the four in the quadrupole) tweezer which is used to attract the micro robot(s) and is positioned accurately via a robotic manipulator [9]. Specific examples of approaches for the control of a microrobot through quadrupole currents in the workspace defined by the end points of the tweezers include the design of an adaptive observer which enables real-time dynamic force sensing and trapping [10], and an adaptive dynamic sliding mode [11] which was used in the context of dielectrophoresis micromanipulation to overcome disturbances on the microrobot.

At the actuation level, and in relation to magnetic microrobots, two main approaches have been proposed in literature for *swarm coordination* [5]: (i) *Torque-based magnetic actuation:* This method [12] generates relatively uniform magnetic fields which apply a moment to magnetized particles, causing them to tumble as they try to align their magnetic moment with that of the field; (ii) *Gradient-based magnetic actuation*: Here, the driving force is generated directly as a result of the variation of the magnetic field around the microrobot. Along these lines, particular examples that include current adjustment in the coils can lead the swarm in a desired directions in a 2-D [13] and 3-D environment [14].

In addition to forces and torques that steer the whole microrobot swarm, there is also local particle-to-particle interaction (e.g. fluidic as well as magnetic interactions) that often be exploited to regulate the swarm's spatial distribution [5], [9]. Paramagnetic nanoparticle swarms have been manipulated to adaptive elliptical formations by exploiting fluidic interactions, and the shape adaptation has been leveraged to enable swarm navigation through confined networks of narrow channels [4]. Recognizing stochastic aspects of the motion of microrobots within an ambient fluid, elements of statistical analysis were used to characterize the distribution of a microrobotic swarm and magnetic field frequency was utilized to control swarm cohesion [15]. It has been confirmed that a rotating gradient-based magnetic field produced by sequentially powering the coils with current can generate attractors within the microrobot workspace at specific loca-

This work was supported by NSF through award no 2234869.

Ioannis Faros and Bert Tanner are with the Department of Mechanical Engineering at the University of Delaware; Email: {ifaros, btanner}@udel.edu

tions determined by the amplitude of the pulses given to the coils [16]. Based on this concept, a sliding mode estimator was subsequently built to estimate the position of the swarm and a robust controller was then designed and interfaced with the estimator to manipulate the swarm in order to follow a pre-specified trajectory [17]. In this case, swarm is steered by repositioning the field attractor dynamically in the workspace by regulating the relative amplitudes of the time-varying pulse-like waveforms of current sent to the coils.

The relation between the coil currents and the location and nature of resulting force vector field equilibrium configurations (locations in the workspace where the force applied to a microrobot placed there is zero) has not been adequately investigated and no analytical expression is available. This fact limits attempts at microrobotic swarm motion planning and control. In the case of a rotating gradient-based magnetic field [16], for instance, the mapping from attractor location to coil current amplitudes is encoded in a back propagation neural network (BPNN). This offers an efficient way to facilitate motion planning but, in general, it does not generalizes to other quadrupole setups and configurations and it offers little insight regarding the nature of the equilibrium points.

This paper thus focuses on quadrupole configurations that utilize piecewise-constant current amplitudes —which are expected to generate static magnetic (and consequently, force) fields, at least during the time interval when the current amplitude levels are maintained— and performs a formal force equilibrium analysis, that enables the prediction of existence, location, and nature of the equilibria in the workspace. Based on this analysis, mathematical conditions are derived to ensure the generation of certain types of field equilibria through application of some specific combination of coil currents.

The remainder of the paper proceeds as follows. Section II defines the objectives and lays out the mathematical framework for the approach. Section III outlines the algorithm for the generation of a desired equilibrium in the quadrupole workspace. Section IV showcases simulation results that support the theoretical analysis presented in the preceding sections. Section V takes a critical look at the outcomes providing an overview that explores possibilities and highlights limitations, and Section VI concludes the paper with the key take-away points.

II. TECHNICAL PRELIMINARIES

Consider a quadrupole of magnetic tweezers and its analytical magnetic force model [6]. First, let the workspace be defined in a 2D Cartesian coordinate system with the origin $(0,0)$ at the center. The four poles (magnetic tweezers) are located at fixed locations at $(0,490)$, $(490,0)$, $(-490,0)$ and $(0,-490)$ respectively. The model for a magnetic force applied to a micro model characterizes the nonlinearity of the magnetic force applied on the micro robot with respect to the currents to the coils and its position in the workspace. The equation that describes this model in a quadratic matrix form is

$$\boldsymbol{F} = k_I \boldsymbol{I}^\intercal \boldsymbol{K}^\intercal \boldsymbol{L}(x,y) \boldsymbol{K} \boldsymbol{I} \ . \tag{1}$$

In the above, $\boldsymbol{F} \in \mathbb{R}^2$ is the two dimensional vector of forces on the microrobot with components along x and y, k_I is the lumped coefficient related to the micro robot and the properties of the magnetic circuit, $\boldsymbol{I} \in \mathbb{R}^4$ is the stack vector of coil currents, and $\boldsymbol{K}$ is a constant matrix that encodes the distribution of magnetic flux:

$$\boldsymbol{K} = \begin{bmatrix} 3/4 & -1/4 & -1/4 & -1/4 \\ 1/4 & 3/4 & -1/4 & -1/4 \\ -1/4 & -1/4 & 3/4 & -1/4 \\ -1/4 & -1/4 & -1/4 & 3/4 \end{bmatrix} \ .$$

Location-dependent matrix $\boldsymbol{L}(x,y) \in \mathbb{R}^{2\cdot 4 \times 2\cdot 4}$ is a 4×4 matrix (with rows and columns indexing the four poles of the quadrupole) where at each element we find a 2-dimensional (x,y) vector. The matrix encodes the outcomes of the gradient operations on the magnetic flux density $\boldsymbol{B}$ that essentially determine the force applied to the microrobot at each location (x,y). Thus if we let $i,j \in \{1,\dots,4\}$ index a pair of poles, and denoting $\boldsymbol{r}_i$ the normalized planar vector from pole i to (x,y) and $\hat{r}_i = \|\boldsymbol{r}_i\|$, we read [6]

$$[\boldsymbol{\ell}]_{i,j} = \frac{1}{\hat{r}_i^3 \hat{r}_j^3} \left[\left(1 - \frac{3\,\hat{\boldsymbol{r}}_i \cdot \hat{\boldsymbol{r}}_j}{\hat{r}_j^2} \right) \hat{\boldsymbol{r}}_j + \left(1 - \frac{3\,\hat{\boldsymbol{r}}_i \cdot \hat{\boldsymbol{r}}_j}{\hat{r}_i^2} \right) \hat{\boldsymbol{r}}_i \right] \ , \tag{2}$$

understanding that $\boldsymbol{r}$ is a function of the microrobot position and thus dropping the dependence on (x,y) from the expression. Separating the x and y component of $[\boldsymbol{\ell}]_{i,j}$ we can split (1) into two scalar equations along the x and y axis:

$$\begin{aligned} F_x &= k_I \boldsymbol{I}^\intercal \boldsymbol{K}^\intercal \boldsymbol{L}_x(x,y) \boldsymbol{K} \boldsymbol{I} \\ F_y &= k_I \boldsymbol{I}^\intercal \boldsymbol{K}^\intercal \boldsymbol{L}_y(x,y) \boldsymbol{K} \boldsymbol{I} \ . \end{aligned} \tag{3}$$

III. APPROACH TO SOLUTION

A. Existence of Force Equilibria

The equilibrium analysis starts with deriving conditions for their existence. In principle, a force equilibrium exists when for a particular nontrivial instance of $\boldsymbol{I}$, the right hand side of (3) vanishes: $F_x = 0 = F_y$.

Note that the right hand side of (3) involves quadratic forms in terms of $\boldsymbol{I}$. One sufficient condition for a force equilibrium, therefore, would be $\boldsymbol{I} \in \mathcal{N}(\boldsymbol{L}_x \boldsymbol{K}) \cap \mathcal{N}(\boldsymbol{L}_y \boldsymbol{K})$. ($\mathcal{N}$ denotes null space.) Matrix $\boldsymbol{K}$ is itself singular, but the case where $\boldsymbol{I} \in \mathcal{N}(\boldsymbol{K})$ is trivial because with this choice of currents, the whole field vanishes. We therefore focus on the null space of $\boldsymbol{L}_x$ and $\boldsymbol{L}_y$, and consider the nonlinear system of equations

$$\det \boldsymbol{L}_x(x,y) = 0 \qquad \det \boldsymbol{L}_y(x,y) = 0$$

that identifies the locations (x,y) where *both* matrices have nontrivial nullspaces. Given (2), it turns out that this happens along the x and y axes. However, these are not the only equilibrium configurations; inspection of (1) indicates that $\boldsymbol{F}$ will also vanish when $\boldsymbol{L}$ rotates the vector it operates on to a direction orthogonal to the one it had originally. These latter

type of equilibria can appear at off-axes locations within the workspace.

B. Location of Force Equilibria

After understanding where and how the equilibria can exist, the next step is to derive sufficient mathematical conditions for their appearance. These conditions will subsequently translate to combinations of coil currents that are capable of generating them at prespecified locations.

For the quadrupole of magnetic tweezers and according to the Gauss's law for magnetism, to ensure that the magnetic flux is always zero [6], meaning that the sum of coil currents should be zero:

$$\begin{bmatrix}1 & 1 & 1 & 1\end{bmatrix}\boldsymbol{I} = 0 \iff \sum_{i=1}^{4} I_i = 0 \ . \tag{4}$$

This constraint can help us project the analysis into a more tractable three-dimensional space. Specifically, define a 4×3 matrix

$$\boldsymbol{S} \triangleq \begin{bmatrix}1 & -1 & -1\\ 0 & 0 & 1\\ 0 & 1 & 0\\ 1 & 0 & 0\end{bmatrix}$$

which spans the orthogonal space to the four-dimensional vector of ones, and let $\boldsymbol{J} \in \mathbb{R}^3$ be a solution of the scalar matrix equation

$$\boldsymbol{SJ} = \boldsymbol{KI} \ . \tag{5}$$

With these definitions, (1) can be written as

$$\boldsymbol{F} = k_I \boldsymbol{J}^\intercal \boldsymbol{S}^\intercal \boldsymbol{L}(x,y)\boldsymbol{SJ} \tag{6}$$

where now $\boldsymbol{S}^\intercal \boldsymbol{L}(x,y)\boldsymbol{S} \in \mathbb{R}^{3\times 3}$. Consequently, (3) is now

$$\begin{aligned} F_x &= k_I \boldsymbol{J}^\intercal \boldsymbol{S}^\intercal \boldsymbol{L_x}(x,y)\boldsymbol{SJ}\\ F_y &= k_I \boldsymbol{J}^\intercal \boldsymbol{S}^\intercal \boldsymbol{L_y}(x,y)\boldsymbol{SJ} \ . \end{aligned} \tag{7}$$

where the quadratic forms involve a three dimensional vector $\boldsymbol{J}$. In this way, after determining the vector $\boldsymbol{J}$ that can produce an equilibrium at some desired location (x_d, y_d), we identify the vector of coil currents $\boldsymbol{I}$ to realize this equilibrium through (5).

Equations (7) are coupled and highly nonlinear with respect to x and y. To solve them for equilibria, say at location (x,y), we define

$$\boldsymbol{A}_x \triangleq \boldsymbol{S}^\intercal \boldsymbol{L}_x(x,y)\boldsymbol{S} \tag{8}$$

and proceed with eigendecomposition for the top part of (7) as follows

$$\begin{aligned} F_x &= \boldsymbol{J}^\intercal \boldsymbol{S}^\intercal \boldsymbol{L}_x(x,y)\boldsymbol{SJ}\\ &= \boldsymbol{J}^\intercal \boldsymbol{A}_x \boldsymbol{J}\\ &= \boldsymbol{J}^\intercal \underbrace{\boldsymbol{U}^\intercal \boldsymbol{\Lambda}_x \boldsymbol{U}}_{\text{eigendecomposition of } \boldsymbol{A}_x} \boldsymbol{J}\\ &\overset{\boldsymbol{z}_x \triangleq \boldsymbol{UJ}}{=} \boldsymbol{z}_x^\intercal \boldsymbol{\Lambda}_x \boldsymbol{z}_x\\ &= \lambda_{x1}|z_{x1}|^2 + \lambda_{x2}|z_{x2}|^2 + \lambda_{x3}|z_{x3}|^2 = 0 \ , \end{aligned} \tag{9}$$

where λ_{xi} are the eigenvalues of $\boldsymbol{A}_x$, arranged along the diagonal of $\boldsymbol{\Lambda}_x$, and z_{xi} the components of $\boldsymbol{z}_x$. Similarly along the y direction, we will have

$$\boldsymbol{A}_y \triangleq \boldsymbol{S}^\intercal \boldsymbol{L}_y(x,y)\boldsymbol{S} \tag{10}$$

and the eigendecomposition gives

$$\begin{aligned} F_y &= \boldsymbol{J}^\intercal \boldsymbol{S}^\intercal \boldsymbol{L}_y(x_d,y_d)\boldsymbol{SJ}\\ &= \boldsymbol{J}^\intercal \boldsymbol{A}_y \boldsymbol{J}\\ &\boldsymbol{J}^\intercal \underbrace{\boldsymbol{P}^\intercal \boldsymbol{\Lambda}_y \boldsymbol{P}}_{\text{eigendecomposition of } \boldsymbol{A}_y} \overset{\boldsymbol{z}_y \triangleq \boldsymbol{PJ}}{=} \boldsymbol{z}_y^\intercal \boldsymbol{\Lambda}_y \boldsymbol{y}_y\\ &= \lambda_{y1}|z_{y1}|^2 + \lambda_{y2}|z_{y2}|^2 + \lambda_{y3}|z_{y3}|^2 = 0 \ . \end{aligned} \tag{11}$$

In (9)–(11), $\boldsymbol{U}$ and $\boldsymbol{P}$ are three-dimensional square matrices whose columns are the eigenvectors of $\boldsymbol{A}_x(x,y)$ and $\boldsymbol{A}_y(x,y)$ respectively, while $\boldsymbol{\Lambda}_x(x,y)$ and $\boldsymbol{\Lambda}_y(x,y)$ are diagonal matrices whose elements are the corresponding eigenvalues. Note that

$$\boldsymbol{J} = \boldsymbol{U^{-1}} \boldsymbol{z}_x = \boldsymbol{P^{-1}} \boldsymbol{z}_y \ . \tag{12}$$

Equations (9)–(12) form a system of two nonlinear and three linear equations, with six unknowns: (z_{xi}, z_{yi}, for $i \in \{1,2,3\}$). In order for (9)–(11) to have acceptable (positive real) solutions, the eigenvalues of $\boldsymbol{A}_x$ and $\boldsymbol{A}_y$ (which are real because the matrices are symmetric) need not to have all the same sign. (Otherwise, the only solution for $\boldsymbol{z}_x$ or $\boldsymbol{z}_y$ is the trivial one.) To examine the sign of those eigenvalues, we need to consider the characteristic polynomials of $\boldsymbol{A}_x$ and $\boldsymbol{A}_y$.

Let the characteristic polynomial of $\boldsymbol{A}_x$ be expressed as

$$\alpha_3 \lambda_{x1}^3 + \alpha_2 \lambda_{x2}^2 + \alpha_1 \lambda_{x3} + \alpha_0 \tag{13}$$

and assume first, without loss of generality, that $\alpha_3 > 0$. Let λ_1, λ_2, λ_3 denote the three roots of (13). Vieta's formulas indicate that

$$\begin{aligned} \alpha_2 &= -\lambda_1 - \lambda_2 - \lambda_3\\ \alpha_1 &= \lambda_1\lambda_2 + \lambda_1\lambda_3 + \lambda_2\lambda_3\\ \alpha_0 &= -\lambda_1\lambda_2\lambda_3 \ . \end{aligned}$$

We need to exclude the possibility of all roots having the same sign. If the roots are all positive, it follows that α_i must satisfy

$$\alpha_2 < 0 \qquad \alpha_1 > 0 \qquad \alpha_0 < 0 \ .$$

If, on the other hand, the roots are all negative

$$\alpha_2 > 0 \qquad \alpha_1 > 0 \qquad \alpha_0 > 0 \ .$$

For the roots to *alternate* in sign, therefore, one of the three following cases must apply:

$$\alpha_3 > 0, \text{ and } \alpha_1 < 0 \text{ or } \begin{cases}\alpha_2 > 0\\ \alpha_1 > 0\\ \alpha_0 < 0\end{cases} \text{ or } \begin{cases}\alpha_2 < 0\\ \alpha_1 > 0\\ \alpha_0 > 0\end{cases} \ . \tag{14}$$

The same analysis can be applied in the case where α_3 is

negative, leading to analogous results:

$$\alpha_3 < 0, \text{ and } \alpha_1 > 0 \text{ or } \begin{cases} \alpha_2 > 0 \\ \alpha_1 < 0 \\ \alpha_0 < 0 \end{cases} \text{ or } \begin{cases} \alpha_2 < 0 \\ \alpha_1 < 0 \\ \alpha_0 > 0 \end{cases} . \quad (15)$$

Note that these coefficients are functions of the microrobot position (x, y). With that in mind, we conclude that if the coefficients $\alpha_i(x, y)$ of the characteristic polynomial (13) satisfy either (14) or (15), then (9) has real solutions for z_{xi} and therefore offer possible solutions for $\boldsymbol{J}$ as follows

$$\boldsymbol{z}_x \equiv \begin{pmatrix} z_{x1} \\ z_{x2} \\ z_{x3} \end{pmatrix} = \boldsymbol{U}\boldsymbol{J} \implies \boldsymbol{J} = \boldsymbol{U}^{-1}\boldsymbol{z}_x \ . \quad (16)$$

Note that (9) specifies 2-parametric solutions for z_{xi}, i.e., taking into account of the squares, one ends with a set of 2D manifolds of possible solutions for z_{xi}.

The same set of conditions (14)–(15) is similarly used on the coefficients of the characteristic polynomial of $\boldsymbol{A}_y$

$$\alpha'_3\lambda^3_{y1} + \alpha'_2\lambda^2_{y2} + \alpha'_1\lambda_{y3} + \alpha'_0$$

to ensure the existence of a feasible solution for (11) and subsequently

$$\boldsymbol{z}_y \equiv \begin{pmatrix} z_{y1} \\ z_{y2} \\ z_{y3} \end{pmatrix} = \boldsymbol{P}\boldsymbol{J} \implies \boldsymbol{J} = \boldsymbol{P}^{-1}\boldsymbol{z}_y \ . \quad (17)$$

Equation (17) yields another pair of 2D manifolds for the possible solutions for $\boldsymbol{z}_y$. Obviously, given that an equilibrium requires $F_x = 0$ *and* $F_y = 0$ for the same (x, y), the solutions for $\boldsymbol{J}$ from (16) and (17) need to match. This means that the solution manifolds of (16) and (17) should intersect so that

$$\boldsymbol{U}^{-1}\boldsymbol{z}_x = \boldsymbol{P}^{-1}\boldsymbol{z}_y \ .$$

When they do, the selected $\boldsymbol{J} = \boldsymbol{U}^{-1}\boldsymbol{z}_x = \boldsymbol{P}^{-1}\boldsymbol{z}_y$ vector can then be used to identify appropriate coil currents $\boldsymbol{I}$ to produce an equilibrium at (x, y) through (5).

In the analysis that follows, we simplify the determination of $\boldsymbol{I}$ by narrowing the solution space for $\boldsymbol{z}_{xi}$: we select $z_{x1} = 1$. This choice renders the number of (nonlinear) algebraic equations in the system equal to the number of unknowns and expedites computation. The numerical solution of the resulting system produces a set of two real solutions for $\boldsymbol{I}$ and two complex (the latter rejected). Each of the two real solutions for $\boldsymbol{I}$ for a given (x, y) can produce an equilibrium at that location, of possibly different nature (i.e., either an unstable node or a saddle). The section that follows expands on the nature of this equilibrium; one key observation, however, is that as long as a case in (14)–(15) applies (which is quite common for an (x, y) in the microrobot's workspace) the particular (x, y) location can be turned into an equilibrium point for the force field, for an appropriate selection of coil currents $\boldsymbol{I}$.

C. Nature of Force Equilibria

In the microrobot's workspace, each distinct solution set $\boldsymbol{I}$ of coil currents obtained through the analysis of Section III-B gives rise to a specific type of equilibrium point. We can characterize the type of equilibrium at a specific location by analyzing the eigenvalues of the Jacobian matrix of the right hand of (3) evaluated at the equilibrium coordinates.

To this end, consider an equilibrium point at coordinates (x_d, y_d), and assume that a combinations of coil currents has been derived as solutions to the system (9)–(12), as described in Section III-B. The Jacobian matrix associated with (3) will be written as

$$\begin{aligned} \boldsymbol{J}_F &= \begin{bmatrix} \frac{\partial F_x}{\partial x} & \frac{\partial F_x}{\partial y} \\ \frac{\partial F_y}{\partial x} & \frac{\partial F_y}{\partial y} \end{bmatrix}_{(x_d, y_d)} \\ &= \begin{bmatrix} \boldsymbol{I}^\intercal\boldsymbol{K}^\intercal\frac{\partial \boldsymbol{L}_x}{\partial x}\boldsymbol{K}\boldsymbol{I} & \boldsymbol{I}^\intercal\boldsymbol{K}^\intercal\frac{\partial \boldsymbol{L}_x}{\partial y}\boldsymbol{K}\boldsymbol{I} \\ \boldsymbol{I}^\intercal\boldsymbol{K}^\intercal\frac{\partial \boldsymbol{L}_y}{\partial x}\boldsymbol{K}\boldsymbol{I} & \boldsymbol{I}^\intercal\boldsymbol{K}^\intercal\frac{\partial \boldsymbol{L}_y}{\partial y}\boldsymbol{K}\boldsymbol{I} \end{bmatrix}_{(x_d, y_d)} . \end{aligned} \quad (18)$$

Extensive sampling of workspace locations and numerical investigation of the eigenvalues of $\boldsymbol{J}_F$ reveals that the solutions for $\boldsymbol{I}$ we obtain through (9)–(12) generally yield either saddles (both solutions of $\boldsymbol{I}$ yield a saddle), unstable node (both solutions of $\boldsymbol{I}$ yield an unstable node) or mixed nodes (where one solution for $\boldsymbol{I}$ can generate a saddle and the other one produce an unstable node). Figure 1 illustrates the different regions of the workspace where it was found that these type of equilibria can be generated.

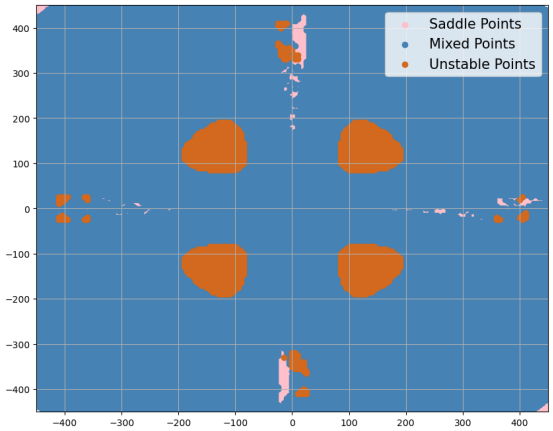

Fig. 1: Classification of possible equilibria generated over a dense grid in the quadrupole workspace.

Turning a point into an attractive node may be appealing as a prospect, given that it offers a straightforward way to accumulate microrobot swarm members. However this setup it is ellusive; the only attractors for the force field appear at the pole locations on the boundary of the workspace. That said, a saddle may as well be the next best thing. As will be demonstrated in the section that follows, the field lines emanating from a force field saddle converge to two of the four poles without diverging significantly from each other along the way. This suggests an expedient way of steering a swarm (from saddle to pole) while preserving its cohesion.

D. How to Generate a Force Equilibrium

This section illustrates the algorithmic process of generating a force field equilibrium in the quadrupole workspace based on the preceding analysis in Section III.

The algorithmic process of equilibrium generation at a point (x_d, y_d) follows these steps:

1) The first step is the evaluation of the coefficients of the characteristic polynomials of $\boldsymbol{A}_x$ and $\boldsymbol{A}_y$, defined in (8) and (10), for the given workspace location.
2) Subsequently, conditions (14)–(15) are checked for both sets of coefficients of the characteristic polynomials of $\boldsymbol{A}_x$ and $\boldsymbol{A}_y$, to ensure that (16) and (17) can yield acceptable solutions for $\boldsymbol{z}_x$ and $\boldsymbol{z}_y$ that agree on $\boldsymbol{J}$.
3) Assuming that the conditions confirm the existence of acceptable solutions, the system of nonlinear algebraic equations (9), (11), and (12) is solved, after reducing the number of unknowns by setting $z_{x1} \coloneqq 1$.
4) If valid solutions for $\boldsymbol{J}$ is identified (two acceptable ones are expected), they is translated into coil current configuration $\boldsymbol{I}$ through (5).
5) The two acceptable solutions for $\boldsymbol{I}$ may produce different types of equilibria. To examine options, the Jacobian $\boldsymbol{J}_F$ is formed through (18) and its eigenvalues calculated to determine the type of equilibrium that can be produced at (x, y) using the two available choices of coil current configurations. Depending on the outcome, a choice of $\boldsymbol{I}$ can then be made.
6) The force vector field is finally generated either directly through (7) through the identified $\boldsymbol{J}$, or through (3) using the calculated $\boldsymbol{I}$. (Note that the physical realization of the field requires $\boldsymbol{I}$.)

The presence of the intended type of equilibrium at the desired workspace configuration is ultimately verified with numerical simulation of the force field.

To illustrate the process, suppose that a force equilibrium at coordinates $(50, 250)$ (in μm) in the workspace is desired. It's nature is to be determined. Going through steps 1)–4) we find the following two possible combinations for coil current configurations:

$$\boldsymbol{I}_{\text{saddle}} = \begin{pmatrix} 1.324 \\ -0.629 \\ -7.184 \\ 6.489 \end{pmatrix} \qquad \boldsymbol{I}_{\text{node}} = \begin{pmatrix} 22.274 \\ -1.018 \\ 33.472 \\ -54.727 \end{pmatrix} .$$

In this case, step 5) produces the following eigenvalues:

$$\begin{pmatrix} \lambda_1 \\ \lambda_2 \end{pmatrix}_{\text{saddle}} = \begin{pmatrix} 1.790 \\ -0.735 \end{pmatrix}$$
$$\begin{pmatrix} \lambda_1 \\ \lambda_2 \end{pmatrix}_{\text{node}} = \begin{pmatrix} 23.490 \\ 15.120 \end{pmatrix}$$

suggesting that one solution for $\boldsymbol{I}$ produces a saddle, whereas the other results in an unstable node. Indeed, Fig. 2 confirms the emergence of these two types of equilibria at the same target location $(x_d, y_d) = (50, 250)$, each produced by the corresponding solution for $\boldsymbol{I}$.

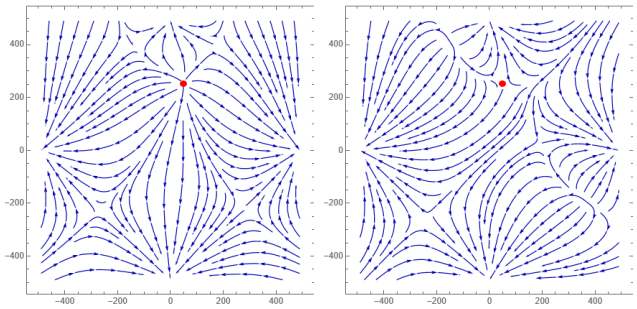

(a) Unstable node. **(b)** Saddle.

Fig. 2: Characterization of a desired equilibrium point at $(50, 250)$ according to the solutions for the coil current vector $\boldsymbol{I}$.

IV. VALIDATION

This section presents simulation results and numerical analysis that supports the theoretical predictions on (a) equilibrium generation in the quadruped force field, and (b) the effect of particular equilibrium placement in the motion behavior of a microrobot swarm. Initially we show a case where the entire swarm can be directed towards a desired pole by spawning a particular equilibrium at its vicinity, and then we explore scenarios where the swam can be split into two subgroups, each moving accordingly to different poles. In addition, we numerically investigate how the nature of the equilibrium point generated in the vicinity of the microrobotic swarm affects affects its cohesion and flocking properties.

For the numerical tests, consider a swarm consisting of ten microrobots, placed at some given location within the quadrupole workspace (see Fig. 3b). By generating a saddle at point $(0, 150)$ (Fig. 3a), which is located slightly above the microrobots' initial locations, we can steer the whole swarm toward the bottom (i.e., at coordinates $(0, -490)$) pole (Fig. 3b) while maintaining its cohesion as a group. This can be achieved because the force field lines converging to poles from saddles tend to stay concentrated and not spread across different directions in the workspace.

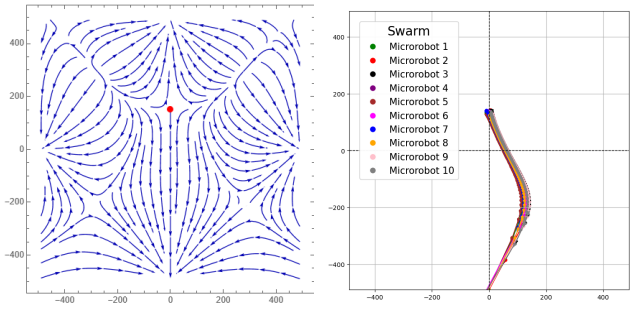

(a) A saddle at $(0, 150)$. **(b)** Swarm converges to a pole.

Fig. 3: When the saddle is located in the vicinity of the swarm it steers it toward a single pole.

Interestingly, with slight adjustments to the selection of the saddle location —or the initial placement of the swarm distribution, as it is the case here— we can obtain group fragmentation and two subgroups to two different quadrupole

poles (Fig. 4b). Which poles will be the designated attractors for the microrobotic swarm is evident in the force vector field plot (Fig. 4a) and can generally be predicted based on the quadrant the equilibrium is generated in and its proximity to the workspace coordinate frame axes.

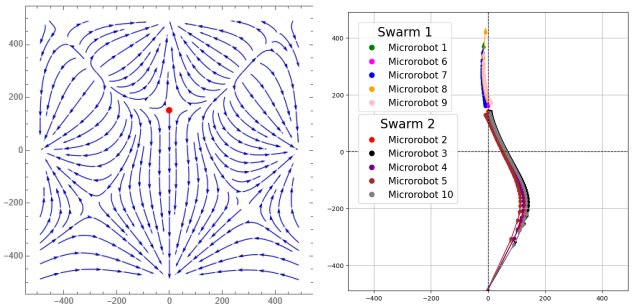

(a) A saddle at $(0, 150)$. **(b)** Swarm splits towards two poles.

Fig. 4: When the saddle is within the swarm, the latter breaks up and its fragments converge to two different poles.

Next, we explore the scenario where the generated equilibrium is an unstable node. To this end, assume that an unstable node is generated among the microrobot swarm members. Then the uniform (along all directions) repulsive influence of the unstable node will cause swarm fragmentation. The number of different fragments produced ultimately depends on the location of the equilibrium relative to the swarm's initial distribution. No cohesion can be expected in this case, although ultimately, as fragments approach poles they disperse less. These effects are showcased in Fig. 5.

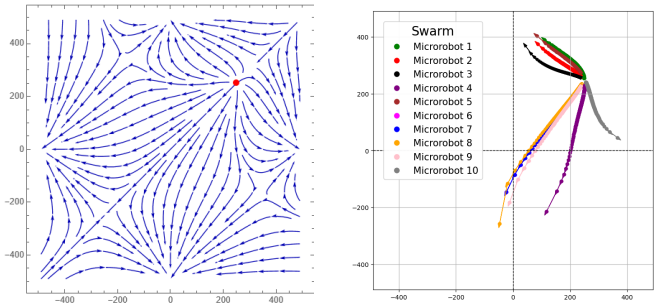

(a) Unstable node at $(250, 250)$. **(b)** Swarm fragmentation.

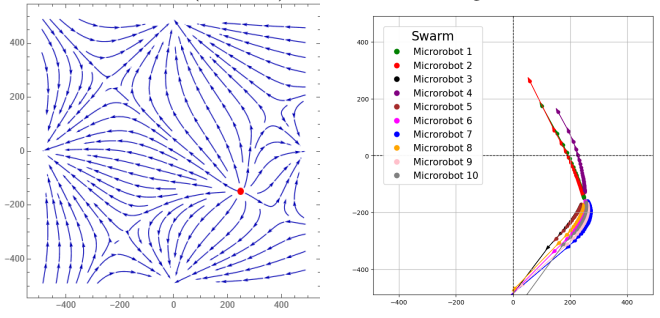

(c) Unstable node at $(250, -150)$. **(d)** Swarm fragmentation.

Fig. 5: Placing an unstable node in or around the initial swarm distribution is likely to cause fragmentation, and the fragments tend to disperse first before converging to poles.

V. DISCUSSION

The nature and the placement of a desired equilibrium point is of the essence for an effective swarm control. Among, the types of equilibria, the saddle point is the particularly of interest as it can lead the entire swarm or its subgroups to desired poles according to its placement with respect to the swarm. To guide the placement of the equilibrium point in the workspace can be divided in four quadrants. The placement of the saddle equilibrium point in one of these quadrants will generate a force vector field with flow lines converging to the two magnetic coil poles which adjacent to that quadrant. If the saddle is positioned on the coordinate axes, then the field flow lines will converge to the magnetic poles on that particular axis (see Fig. 4). External positioning of the quadrupole (see e.g. [9]) can potentially make those poles coincide with desired destinations or waypoints for the microrobotic swarm.

Depending on whether one desires to keep the whole swarm together or break it into (two) groups, they can strategically position the saddle around or within the swarm initial distribution. In the former case, the swarm will be steered toward the magnetic pole attractor that faces the swarm. In the latter case, the swarm will split into two groups and each will follow a path toward one of the two attractors. In both cases, the swarm will maintain its cohesion during its convergence phase.

Only magnetic poles can become attractors, and in a quadrupole configuration those attractors will appear on the boundary of the microrobotic workspace. It can be envisioned that a robotic device, e.g. a manipulator [9] can reposition those magnetic poles, potentially in a sequential manner, thus enabling microrobotic swarm large scale motion through waypoint navigation.

VI. CONCLUSIONS

Analytical investigation of the mathematical mapping between coil currents and the generated force field on magnetic microparticles within a quadrupole workspace configuration reveals that force equilibria can be generated anywhere in the workspace by appropriate choice of coil currents. Subsequent theoretical and numerical analysis of the resulting force field Jacobian matrices indicates that the generated equilibria are typically saddles or unstable nodes. Of these two types, saddles appear to be useful for magnetic microrobot swarm control: depending on the placement of the saddle with respect to the microrobot swarm initial distribution, the swarm can be steered toward one of the four magnetic poles, while the group maintains cohesion during convergence. What is more, it is seen that placing the saddle within the initial distribution has the effect of splitting the swarm in two and directing the two subgroups toward two different magnetic poles. These results potentially open a new pathway to microrobot swarm control, which together with online quadrupole reconfiguration can potentially enable point-to-point or point-to-multiple-points microrobot swarm control.

REFERENCES

[1] U. Kei Cheang, K. Lee, A. A. Julius, and M. J. Kim, "Multiple-robot drug delivery strategy through coordinated teams of microswimmers," *Applied Physics Letters*, vol. 105, no. 8, p. 083705, 2014.

[2] M. P. Kummer, J. J. Abbott, B. E. Kratochvil, R. Borer, A. Sengul, and B. J. Nelson, "Octomag: An electromagnetic system for 5-dof wireless micromanipulation," *IEEE Transactions on Robotics*, vol. 26, no. 6, pp. 1006–1017, 2010.

[3] B. J. Nelson, I. K. Kaliakatsos, and J. J. Abbott, "Microrobots for minimally invasive medicine," *Annual Review of Biomedical Engineering*, vol. 12, no. 1, pp. 55–85, 2010.

[4] J. Yu, L. Yang, X. Du, H. Chen, T. Xu, and L. Zhang, "Adaptive pattern and motion control of magnetic microrobotic swarms," *IEEE Transactions on Robotics*, vol. 38, no. 3, pp. 1552–1570, 2021.

[5] L. Yang, J. Yu, S. Yang, B. Wang, B. J. Nelson, and L. Zhang, "A survey on swarm microrobotics," *IEEE Transactions on Robotics*, vol. 38, no. 3, pp. 1531–1551, 2022.

[6] Z. Zhang, K. Huang, and C.-H. Menq, "Design, implementation, and force modeling of quadrupole magnetic tweezers," *IEEE/ASME Transactions on Mechatronics*, vol. 15, no. 5, pp. 704–713, 2010.

[7] S. Das, E. B. Steager, M. A. Hsieh, K. J. Stebe, and V. Kumar, "Experiments and open-loop control of multiple catalytic microrobots," *Journal of Micro-Bio Robotics*, vol. 14, pp. 25–34, 2018.

[8] Z. Zhang, Y. Huang, and C.-H. Menq, "Actively controlled manipulation of a magnetic microbead using quadrupole magnetic tweezers," *IEEE Transactions on Robotics*, vol. 26, no. 3, pp. 531–541, 2010.

[9] X. Wang, T. Wang, G. Shan, J. Law, C. Dai, Z. Zhang, and Y. Sun, "Robotic control of a magnetic swarm for on-demand intracellular measurement," in *Proceedings of the International Conference on Robotics and Automation*, 2020, pp. 11 385–11 391.

[10] Y. Huang, P. Cheng, and C.-H. Menq, "Dynamic force sensing using an optically trapped probing system," *IEEE/ASME Transactions on Mechatronics*, vol. 16, no. 6, pp. 1145–1154, 2010.

[11] H. Luo, W. Sun, and J. T. Yeow, "Modelling and adaptive dynamic sliding mode control of dielectrophoresis-based micromanipulation," *Transactions of the Institute of Measurement and Control*, vol. 40, no. 1, pp. 122–134, 2018.

[12] J. J. Abbott, K. E. Peyer, M. C. Lagomarsino, L. Zhang, L. Dong, I. K. Kaliakatsos, and B. J. Nelson, "How should microrobots swim?" *The International Journal of Robotics Research*, vol. 28, no. 11-12, pp. 1434–1447, 2009.

[13] D. De Lanauze, O. Felfoul, J.-P. Turcot, M. Mohammadi, and S. Martel, "Three-dimensional remote aggregation and steering of magnetotactic bacteria microrobots for drug delivery applications," *The International Journal of Robotics Research*, vol. 33, no. 3, pp. 359–374, 2014.

[14] D. Loghin, C. Tremblay, M. Mohammadi, and S. Martel, "Exploiting the responses of magnetotactic bacteria robotic agents to enhance displacement control and swarm formation for drug delivery platforms," *The International Journal of Robotics Research*, vol. 36, no. 11, pp. 1195–1210, 2017.

[15] L. Yang, J. Yu, and L. Zhang, "Statistics-based automated control for a swarm of paramagnetic nanoparticles in 2-d space," *IEEE Transactions on Robotics*, vol. 36, no. 1, pp. 254–270, 2019.

[16] L. Xing, D. Li, H. Cao, L. Fan, L. Zheng, L. Zhang, and D. Sun, "A new drive system for microagent control in targeted therapy based on rotating gradient magnetic fields," *Advanced Intelligent Systems*, vol. 4, no. 9, p. 2100214, 2022.

[17] H. Cao, L. Xing, J. Hu, H. Mo, and D. Sun, "Automated control of microparticle swarm in a rotating gradient-based magnetic field," *IEEE Transactions on Automation Science and Engineering*, pp. 1–10, 2024.